On-Chip Detection of Orbital Angular Momentum Beam by Plasmonic Nanogratings

Ji Chen, Xi Chen, Tao Li, and Shining Zhu*

Thanks to the unlimited orthogonal states, the orbital angular momentum (OAM) light is widely accepted as a promising carrier for high information multiplexing in optical communications, in which the OAM detection is an important issue. To keep up with the ever-growing demand for compact integration, here, a plasmonic grating is employed to spatially couple the OAM modes into two separated propagating surface plasmon polariton (SPP) beams with different splitting angles. These splitting angles are found to strongly rely on the topological charges of the incident beams and are insensitive to the specific location of the OAM beam illumination, which provides an intuitive detection of the OAM modes without particular alignment. Besides, a further unidirectional SPP launching from the OAM beam is also achieved by a particular composite grating. With such composite grating, both the topological charge value and sign of OAM beam in a single measurement can be detected. Our results provide a convenient method for alignment-free OAM detection by a compact device, and would inspire more multiplexing applications in nanophotonics.

1. Introduction

Orbital angular momentum (OAM) light is well known for its helical wavefront of $\exp(il\phi)$, which carries an OAM of $l\hbar$ per photon (where l is referred to the topological charge),[1] and has a phase singularity at the center resulting in a ring-shaped vortex beam. Due to these unique aspects, the OAM beam has been intensively studied toward its promising applications in optical tweezers,[2] nonlinear optics,[3] quantum information processing,[4,5] optical data storage and transmission,[6–10] and so on. In principle, the information encoding by dimension of OAM would have infinite high capacity, and hence the OAM beam is of great importance in multiplexing optical signals in communication systems.[11,12] To correctly obtain the information carried by multiplexed OAM modes, an efficient approach to detect the OAM modes is required at the terminal of a communication system. Several methods have already been proposed to detect the OAM modes, for example, forked holographic structures,[13,14] well-arranged nanorod metasurface,[15] concentric semi-ring shaped nanoslits,[16] optical elements with log-polar transformation,[17–20] or integrated photonic circuit.[21] The common principle of these methods is converting the OAM modes into measurable signals when the beam is aligned to the right local place of the detection structure, and the devices are usually space consuming due to the diffraction process. Since the compact integration has always been the pursuit of optical processing and communication,[22–26] how to further minimize and stabilize the OAM detector in a more robust way are still what the people are working for nowadays.

In this article, we propose a new technique for detection of OAM modes without the strict alignment between incident light and the structured sample. It is implemented by coupling the OAM beam into two separated SPP beams according to a well-designed in-plane wave vector (k-vector) matching process by a nanograting on a metal surface. According to the relation between the splitting angle of SPP beams and the topological charge of the vortex beam, one can detect the OAM property. Since the k-vector matching process between the reciprocal vector of grating and azimuth vector of OAM is independent of the local place of the structure, this detection process is quite robust and without particular alignment, which will be helpful in efficient OAM detection. Moreover, by combining two types of gratings with the engineered k-vector matching process, we successfully convert vortex beams into a unidirectional propagation SPP beam, which enriches functionality of the OAM-based devices. Therefore, this design is developed to detect both the value and the sign of a topological charge in a single process. This on-chip detection for OAM modes suggests new possibilities in integrated nanophotonic designs and devices.

2. Principle of OAM Modes Discrimination

Here, the well-known Laguerre–Gaussian beam is used,[27] which is a vortex beam with a topological charge of l. By

J. Chen, X. Chen, Prof. T. Li, Prof. S. Zhu
National Laboratory of Solid State Microstructures
College of Engineering and Applied Sciences
Nanjing University
Nanjing 210093, China
E-mail: taoli@nju.edu.cn
J. Chen, X. Chen, Prof. T. Li, Prof. S. Zhu
Collaborative Innovation Center of Advanced Microstructures
Nanjing University
Nanjing 210093, China

The ORCID identification number(s) for the author(s) of this article can be found under https://doi.org/10.1002/lpor.201700331

DOI: 10.1002/lpor.201700331

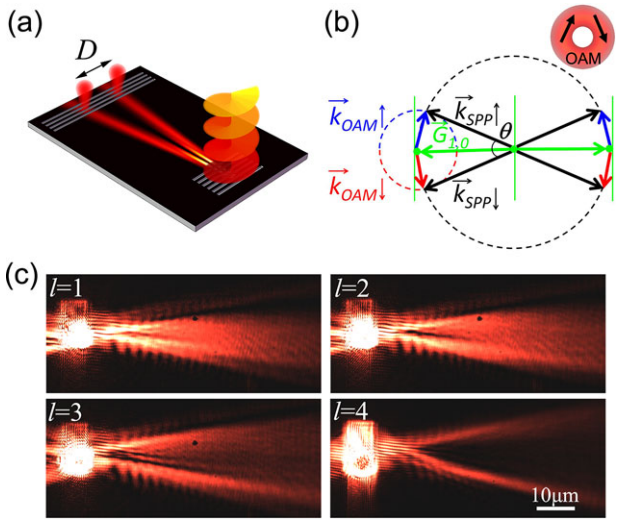

Figure 1. The strategy of on-chip detection of OAM modes. a) Schematics of the OAM detection process. b) The vector analysis of the conversion from OAM beam to SPPs, which indicates two couples of split SPP beams will be launched at both sides of the gratings. c) The LRM recorded SPP waves (only one side is shown) converted from OAM illuminations with different topological charges ($l = 1, 2, 3, 4$).

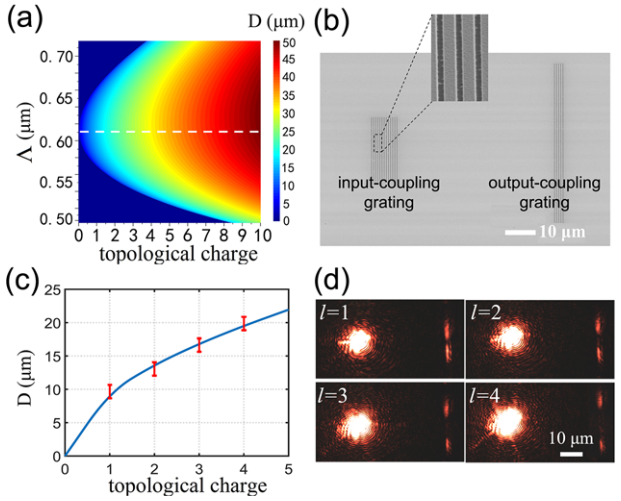

Figure 2. Analyses of separate SPP beams for OAM discrimination. a) The calculated diagram of separation (D) value as the function of OAM topological charge (l) and grating periods (Λ). b) The SEM image of the sample with $\Lambda = 610$ nm. Inset is a zoom-in image. c) The blue curve is the calculating relation of the D and l, in condition of OAM illumination with $\lambda_0 = 633$ nm (corresponding to the dashed white line in (a)). The red error bars are the experimental data (from (d)) of spot distances of SPP scattering in output-coupling grating. d) The optical microscopy images of input and output-coupling of SPPs with respect to different OAM topological charges ($l = 1, 2, 3, 4$).

illuminating the vortex beam onto a grating structure with a period of Λ, particular SPP waves will be excited in two symmetric directions according to the k-vector compensations, as schematically shown in **Figure 1**a. This conversion process can be predicted by the 2D wave vector analysis in reciprocal space (see Figure 1b), where $\vec{G}_{1,0}$ is the reciprocal vector of grating expressed as $\vec{G}_{1,0} = \frac{2\pi}{\Lambda}$, while $\vec{k}_{\mathrm{OAM}}$ and $\vec{k}_{\mathrm{SPP}}$ are wave vectors of the azimuth component of the incident vortex beam and the converted SPP wave, respectively. Note that the vortex beam is illuminated normally, and only the azimuthal wave vector of the vortex beam contributes to the conversion process. Then we have $|\vec{k}_{\mathrm{OAM}}| = \frac{l\pi}{2r(l)}$, where $r(l)$ is the effective radius of the vortex beam with topological charge of l. The conversion process will occur when the k-vector matching condition is satisfied as

$$\vec{k}_{\mathrm{SPP}} - \vec{k}_{\mathrm{OAM}} = \vec{G}_{1,0} \tag{1}$$

From Figure 1b, it can be seen at each side of the grating structure, there will be two k-vector matching conditions, which indicates two couples of separate SPP waves can be launched with the same splitting angle of θ due to the symmetric design. Note that according to the nature of angular momentum, the k_{OAM} has all in-plane directions that can be selected out for the k-vector matching, as indicated in the inset of Figure 1b. It is easy to retrieve the splitting angle as

$$\theta = 2\arcsin\left(\frac{k_{\mathrm{OAM}}}{G_{1,0}}\right) \tag{2}$$

According to Equation (2), we find that different topological charges correspond to different k_{OAM}, and result in different splitting angle. In principle, the larger l gets, the larger θ is. In the experiments for the proof of concept, we employed a home-built leakage radiation microscopy (LRM), which was widely used in SPP beam observation,[28–30] to characterize the propagation of launched SPP waves on metal surface. As the launched split SPP beams at the two sides are symmetric, only the one side results are shown for simplicity (Figures 1c and 2b). Figure 1c shows the observed results by illumination of vortex beams with different topological charges ($l = 1, 2, 3, 4$). The experimental details will be presented in the next section. Here, we would like to take a glance at the experimental results. It can be easily observed that as the topological charge gets larger, the two launched SPP waves will be more separated with an enlarged splitting angle, which phenomenologically agrees with our theoretical prediction.

To precisely analyze the separation degree, an output-coupling grating was then introduced with a distance (L) to the input-coupling grating. Then the two branches of SPP beams will be scattered out at two local spots on the output-coupling grating with a separate distance D, which can be retrieved as $D = L\tan\theta$. According to Equation (2), we can calculate the detailed D values with respect to different grating periods and topological charges, as the calculation results shown in **Figure 2**a. It does provide us a quantitative measurement of the topological charge for a given wavelength.

3. Experimental Detection of OAM Modes

Figure 2b displays the scanning electric microscope (SEM) image of the sample with input-coupling and output-coupling gratings,

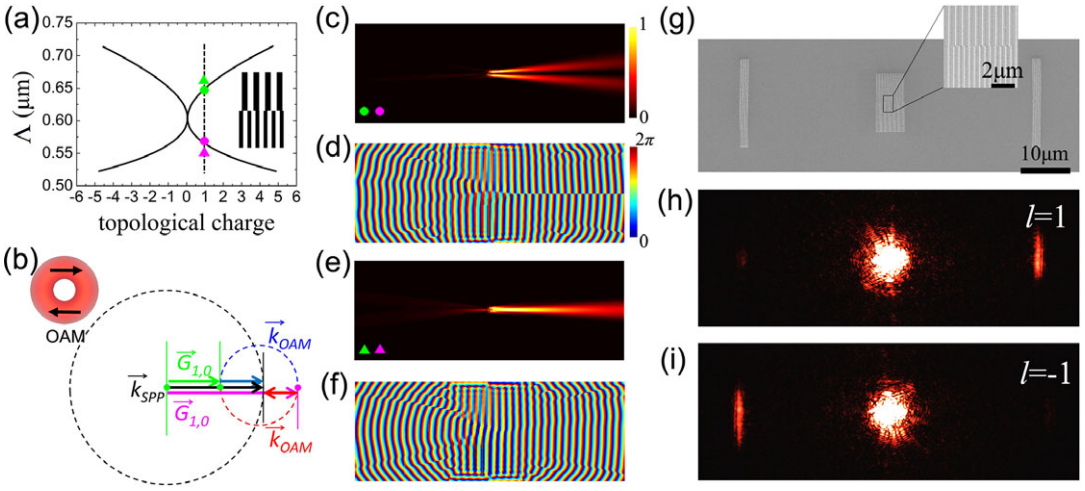

Figure 3. Design of unidirectional SPP coupling. a) The calculated critical curve with respect to period of gratings and topological charges for the condition of unidirectional SPP coupling. Two circles represent the periods of gratings selected right on the curve, while the two triangles are two loose conditions with the periods close to the critical curve. The inset image is the scheme of composite input-coupling structure. b) Wave vector analysis of the two critical states. c,d) The calculated intensity and phase distributions of the coupled SPP waves, respectively, with the grating periods selected as the two circles in (a). e,f) The calculated results with grating periods selected as the two triangles. g) The SEM image of the sample with two output-coupling gratings at the two sides of the composite input-coupling grating. The inset figure is the zoom-in image of the input-coupling grating. The observation results of unidirectional SPP launchings with the illuminating OAM beams of h) $l = 1$ and i) $l = -1$, respectively.

in which the zoom-in image shows the details of the gratings. The whole device size including input and output-coupling grating is about $70 \times 40\ \mu m^2$. In the sample, L is set as 60 μm and the input- and output-coupling gratings are all designed with the same period of 610 nm, which is equivalent with the corresponding SPP wavelength coupled from the He–Ne laser ($\lambda_0 = 633$ nm). All the structures are fabricated by the etching of Focus Ion Beam (FIB, dual-beam FEI Helios 600i) on a 60 nm thick silver film with a silica substrate. According to these parameters, the separate distance D can be retrieved from previous calculation at the grating period of 610 nm (see the white dashed line in Figure 2a), which is displayed as a blue curve in Figure 2c. In our optical characterization, the scattered optical signals were recorded by CCD when a series of OAM vortex beams incident onto the input-coupling grating with different topological charges ($l = 1, 2, 3, 4$), as shown in Figure 2d. Then the experimental data of D can be extracted from these images and plotted in Figure 2c (with error bars), which agree well with the theoretical curve. In this experiment, the incident vortex beams with different topological charges are generated by a reflective-type spatial light modulator (SLM, HOLOEYE GAEA-VIS-036) with a Gaussian beam input (He–Ne laser at $\lambda_0 = 633$ nm). The observation of SPP waves on metal surface (Figure 1c) are characterized by a home-built LRM system. The out-coupling SPP spots (Figure 2d, and the following Figure 4b,c) are characterized by a microscope system with an objective of NA = 1.42.

Since the grating structures are uniform, the k-vector matching condition will be always satisfied as long as the input-coupling grating is illuminated, which leads to very loose alignment of the incident vortex beam and the structures in the overall process. This approach indicates great advantage especially in devices with ultrasmall scale, because it will improve the fault tolerance of the OAM detection process and possibly accelerate the detection speed.

4. Unidirectional Coupling of OAM Modes

Such an OAM detection structure was implemented using a uniform plamsonic nanograting with a mirror symmetry, which actually couples the incident OAM beam into two sets of split SPP beams at both sides of the structure. By further analyzing the k-vector matching process, we would possibly break this symmetry by designing a composite grating structure with two different periods. This design will unidirectionally couple the OAM mode into SPP wave propagating on one side, which is of much importance in plasmonic devices [31–33] In Equation (2), when we set θ as zero, two separately launched SPP waves will be degenerated that tends to combine them into a single SPP beam. Based on this critical condition, it was calculated out with a relation between the period of Λ and topological charge of l that satisfies the condition of $\theta = 0$. **Figure 3**a shows the calculated critical curve, from which we can find that there will be always two Λs that satisfy the condition with respect to a certain nonzero topological charge. The critical state for each topological charge can be intuitively illustrated in the wave vector analysis, as shown in Figure 3b, where the three vectors $\vec{k}_{SPP}$, $\vec{k}_{OAM}$, and $\vec{G}_{1,0}$ are collinear. These two satisfied $\vec{G}_{1,0}$ (up and down parts) plus two opposite $\vec{k}_{OAM}$ can synthesize two identical $\vec{k}_{SPP}$ in the same direction. Therefore, with a composite grating containing two different Λs (like the inset in Figure 3a), the incident OAM beam will unidirectionally couple into an SPP wave to the right side as long as the beam illuminates equally on two grating parts.

Before carrying out the experiments, we first use the 2D Huygens–Fresnel principle to simulate the coupling process, by which the versatile SPP beams have been successfully designed in previous works.[28–30] The periods of the two composite gratings are chosen as the green and purple circle symbols on the

critical curve in Figure 3a. Figure 3c shows the calculation result, from which it is observed that only the SPP waves launched toward one side agree well with the wave vector analysis. However, it is also evident that the two launched SPPs still split into two beams, which will somewhat degrade the beam quality. By careful analyses, the phenomenon is found resulting from the phase difference of the two launched SPP waves, as shown in Figure 3d. To solve this problem, two quasi-critical states are selected near the critical curve with the same propagating phase (see the green and purple triangle symbols in Figure 3a). The simulation results are shown in Figure 3e,f, where a merged single SPP beam propagating toward the right side is well demonstrated and the phases are identical for both the upper and lower parts. This simulation has predicted a superb unidirectional launching of SPP even in this quasi-critical condition. If the topological charge of the OAM beam switches to the opposite one, the whole analysis is still valid and predicts a reversed SPP launching. Therefore, by changing the sign of the topological charge of the OAM beam, the launched SPP wave propagation can be controlled.

In these experiments, we fabricated two output-coupling gratings at two sides of the input-coupling structure, as shown in Figure 3g. The input-coupling structure is a composite grating with two periods of 660 and 550 nm in the upper and lower parts, respectively, according to our calculations. Figure 3h,i display the optical detection of the unidirectional SPP launchings with the illuminating OAM beams of $l = 1$ and -1, respectively. It can be clearly observed that the composite grating can unidirectionally convert the OAM beams into one side propagating SPP, which agrees well with our theoretical prediction. To examine the performance of unidirectionality we further analyzed the extinction ratio (the weaker over the stronger), which are both smaller than 0.15 indicating good unidirectional property.

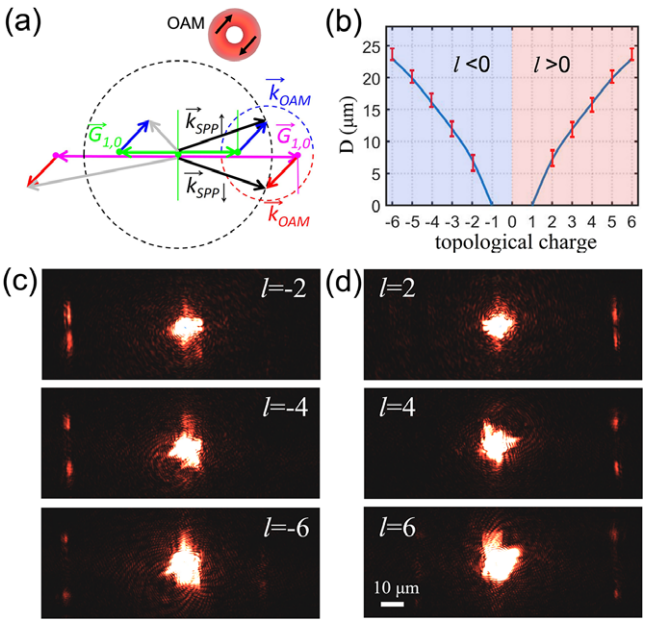

Figure 4. Unidirectionally coupling of OAM modes with $|l|>1$. a) Wave vector analysis of the unidirectionally coupling process, when OAM light illuminated on the coupling structure which has the same parameters with the structure shown in Figure 3g. b) The blue curves are the calculating relations of separation D and topological charges *l*. The red error bars are the experimental data of spot distances extracted from the microscopy images, some of which are shown in (c) for negative ($l = -2, -4, -6$) topological charges, and (d) for positive ($l = 2, 4, 6$) ones.

5. Complete Measurement of Topological Charge

So far, two types of grating designs were proposed to discriminate either the topological charge value or the sign of the incident OAM beam. It is quite possible to combine them together to achieve a full measurement of the topological charges including the value and sign at the same time. Here, we take further investigations on SPP coupling property by illuminating OAM modes with larger topological charge values ($|l| > 1$) onto the same composite grating as designed in Section 5 (with two gratings of $\Lambda = 660$ nm and 550 nm). **Figure 4**a schematically shows the wave vector analysis, where three vectors $\vec{k}_{SPP}$, $\vec{k}_{OAM}$, and $\vec{G}_{1,0}$ are no longer collinear. However, these k-vector matching conditions will only be satisfied at one side of the structure as the up-and-down symmetry is broken, resulting in two split SPP beams at the right side (in the case of Figure 4a). Only when the sign of the incident OAM topological charge is switched, the coupling conditions will be satisfied at the opposite side. It rightly indicates using such kind of composite grating can definitely distinguish the topological charge value by the splitting angle and its sign by coupling direction.

By further calculation, we get the relations between the separation distance (*D*) of the split SPP beams and the topological charges with both negative and positive signs. The relations are shown as the two blue curves in Figure 4b. In experiment, the different separation distances (*D*) were also detected by the CCD, when a series of OAM beams with different topological charges ($l = \pm1, \pm2, \pm3, \pm4, \pm5, \pm6$) incident onto the composite grating (as in Figure 3g). The red error bars in Figure 4b are the experimental data of the separation distances D, which agree well with the calculated curves. Figure 4c,d shows the optical microscopy images of unidirectional coupling of SPPs with respect to OAM beam with negative topological charges ($l = -2, -4, -6$) and positive ones ($l = 2, 4, 6$), respectively. From these results, we can see by using this composite grating structure, both the values and signs of the topological charges can be discriminated at the same time.

In this article, we did not provide the experimental results with respect to $|l| > 6$, though the method should be valid in principle. In practical experiments, when $|l|$ gets larger, the intensity of the launched SPP waves decreases as, on the one hand, matching degree lowers down. On the other hand, the difference of separation distances with larger charge values will be smaller, which also brings difficulty in discriminating the charges. According to our experiments, OAM beams with $|l| < 10$ can be well discriminated. Additionally, we would like to explain that this method is not valid for the OAM beams with fractional topological charge,[34,35] since they are not stable beams where the variable discontinuity in phase will dramatically influence the coupled SPP beam profiles and destroy the measurement.

6. Conclusion

In summary, we proposed and demonstrated a brand new approach to discriminate the topological charges of a spatial OAM beam, by converting it into two separated propagating SPP beams with nanogratings. The separation degree of the SPP waves, which reflects the topological charge, does not depend on the illuminating position of the OAM beam, which indicates this process is alignment-free. By using a composite grating structure with different periods, unidirectional coupling of OAM modes was also successfully realized, which can be switched by the sign of the topological charge of the incident OAM beam. Moreover, based on such a composite grating, a full detection of topological charge value and sign is implemented within a single device. Our results significantly provide new strategies of alignment-free OAM detection and unidirectional SPP coupling, which would possibly advance new optical designs associated with OAM beams and inspire new functionalities as the high-dimensional OAM being used.

Acknowledgements

T.L. supervised the research. T.L., J.C., and X.C. conceived the idea and designed the experiment. X.C. performed the numerical calculations. J.C. fabricated the sample, and performed the optical analyses with assistance from X.C. T.L. and J.C. analyzed the results and wrote the paper. All authors contributed to the discussions. The authors thank Dr. Peng Chen and Dr. Rui Ni for their valuable discussion and Dr. Qianjin Wang for his assistance in sample fabrication. This work is supported by National Key R & D Program of China (2017YFA0303700, 2016YFA0202103), National Natural Science Foundation of China (Nos. 11674167, 11621091), and PAPD from the government of Jiangsu Province. T.L. thanks the support from Dengfeng Project B of Nanjing University.

Conflict of Interest

The authors declare no conflict of interest.

Keywords

detection, surface plasmon polariton, topological charge, vortex beam

Received: December 12, 2017
Revised: April 29, 2018
Published online: July 3, 2018

[1] L. Allen, M. W. Beijersbergen, R. J. C. Spreeuw, J. P. Woerdman, *Phys. Rev. A* **1992**, *45*, 8185.
[2] M. Padgett, R. Bowman, *Nature Photon*. **2011**, *5*, 343.
[3] D. S. Ding, Z. Y. Zhou, B. S. Shi, X. B. Zhou, G. C. Guo, *Opt. Lett.* **2012**, *37*, 3270.
[4] V. D'Ambrosio, E. Nagali, L. Marrucci, F. Sciarrino, *Quantum Opt. II* **2012**, *8440*, 84400.
[5] X. B. Zhou, W. Mathis, *Phys. Rev. A.* **2005**, *71*, 042324.
[6] R. Voogd, M. Singh, J. Braat, *Proc. SPIE* **2004**, *387*, 5380.
[7] G. Gibson, J. Courtial, M. J. Padgett, *Opt. Express* **2004**, *12*, 5448.
[8] J. Wang, J.-Y. Yang, I. M. Fazal, N. Ahmed, Y. Yan, H. Huang, Y. Ren, Y. Yue, S. Dolinear, M. Tur, A. E. Willner, *Nature Photon*. **2012**, *6*, 488.
[9] N. Bozinovic, Y. Yue, Y. Ren, M. Tur, P. Kristensen, H. Huang, A. E. Willner, S. Ramachandran, *Science* **2013**, *28*, 1545.
[10] H. Huang, G. Xie, Y. Yan, N. Ahmed, Y. Ren, Y. Yue, D. Rogawski, M. J. Willner, B. I. Erkmen, K. M. Birnbaum, S. J. Dolinear, M. P. J. Lavery, M. J. Padett, M. Tur, A. E. Willner, *Opt. Lett.* **2014**, *39*, 197.
[11] S. N. Khonina, V. V. Kotlyar, R. V. Skidanov, V. A. Soifer, P. Laakkonen, J. Turunen, *Opt. Commun.* **2000**, *175*, 301.
[12] M. Padgett, J. Arlt, N. Simpson, L. Allen, *Am. J. Phys.* **1996**, *64*, 77.
[13] P. Genevet, J. Lin, M. A. Kats, F. Capasso, *Nature Commun*. **2012**, *3*, 1278.
[14] P. Chen, S.-J. Ge, L.-L. Ma, W. Hu, V. Chigrinov, Y.-Q. Lu, *Phys. Rev. Appl.* **2016**, *5*, 044009.
[15] M. Q. Mehmood, S. Mei, S. Hussain, K. Huang, S. Y. Siew, L. Zhang, T. Zhang, X. Ling, H. Liu, J. Teng, A. Danner, S. Zhang, C.-W. Qiu, *Adv. Mater.* **2016**, *28*, 2533.
[16] S. Mei, K. Huang, H. Liu, F. Qin, M. Q. Mehmood, Z. Xu, M. Hong, J. Teng, A. Danner, C.-W. Qiu, *Nanoscale* **2016**, *8*, 2227.
[17] G. C. G. Berkhout, M. P. J. Lavery, J. Courtial, M. W. Beijersbergen, M. J. Padgett, *Phys. Rew. Lett.* **2010**, *105*, 153601.
[18] M. Mirhosseini, M. Malik, Z. Shi, R. W. Boyd, *Nature Commun*. **2013**, *4*, 2781.
[19] J. Zhou, W. Zhang, L. Chen, *Appl. Phys. Lett.* **2016**, *108*, 111108.
[20] S. Zheng, J. Wang, *Sci. Rep*. **2017**, *7*, 40781.
[21] G. Rui, B. Gu, Y. Cui, Q. Zhan, *Sci. Rep*. **2016**, *6*, 28262.
[22] N. Shitrit, I. Bretner, Y. Gorodetski, V. Kleiner, E. Hasman, *Nano Lett*. **2011**, *11*, 2038.
[23] N. Shitrit, S. Nechayev, V. Kleimer, E. Hasman, *Nano Lett*. **2012**, *12*, 1620.
[24] D. Lin, P. Fan, E. Hasman, M. I. Brongersma, *Science* **2014**, *345*, 298.
[25] M. Q. Mehmmod, H. Liu, K. Huang, S. Mei, A. Danner, B. Luk'yanchuk, S. Zhang, J. Teng, S. A. Maier, C.-W. Qiu, *Laser Photonics Rev*. **2015**, *9*, 674.
[26] J. Chen, T. Li, S. Wang, S. Zhu, *Nano Lett*. **2017**, *17*, 5051.
[27] A. M. Yao, M. J. Padgett, *Adv. Opt. Photon*. **2011**, *3*, 161.
[28] L. Li, T. Li, S. M. Wang, C. Zhang, S. N. Zhu, *Phys. Rev. Lett.* **2011**, *107*, 126804.
[29] L. Li, T. Li, S. M. Wang, S. N. Zhu, *Phys. Rev. Lett.* **2013**, *110*, 046807.
[30] J. Chen, L. Li, T. Li, S. N. Zhu, *Sci. Rep*. **2016**, *6*, 28926.
[31] A. Baron, E. Devaux, J.-C. Rodier, J.-P. Hugonin, E. Rousseau, T. W. Ebbesen, P. Lalanne, *Nano Lett*. **2011**, *11*, 4207.
[32] L. Huang, X. Chen, B. Bai, Q. Tan, G. Jin, T. Zentgraf, S. Zhang, *Light: Sci. Appl.* **2013**, *2*, e70.
[33] J. Lin, B. Mueller, Q. Wang, G. Yuan, N. Antoniou, X.-C. Yuan, F. Capasso, *Science* **2013**, *340*, 331.
[34] J. B. Götte, K. O'Holleran, D. Preece, F. Flossmann, S. Franke-Arnold, S. M. Barnett, M. J. Padgett, *Opt. Express* **2008**, *16*, 993.
[35] K. Huang, H. Liu, S. Restuccia, M. Q. Mehmood, S.-T. Mei, D. Giovannini, A. Danner, M. J. Padgett, J.-H. Teng, C.-W. Qiu, *Light: Sci. Appl.* **2018**, *7*, e17156.